Mon. Not. R. Astron. Soc. 000, 1–6 (1999) Printed 9 March 1999 (MN LATEX style file v1.4)

C II 158 μm observations of a sample of late-type galaxies from the Virgo cluster

K. J. Leech,[1⋆] H.J. Völk,[2] I. Heinrichsen,[1,2,4] H. Hippelein,[3] L. Metcalfe,[1] D. Pierini,[2] C.C. Popescu,[2,5] R.J. Tuffs[2] and C. Xu[4]

[1] *ISO Data Centre, Astrophysics Division, ESA, Villafranca, Spain*
[2] *Max-Planck-Institut für Kernphysik, Heidelberg, Germany*
[3] *Max-Planck-Institut für Astronomie, Heidelberg, Germany*
[4] *IPAC, Caltech, USA*
[5] *The Astronomical Institute of the Romanian Academy, Str. Cuțitul de Argint 5, 75212 Bucharest, Romania*

Accepted 1988 December 15. Received 1988 December 14; in original form 1988 October 11

ABSTRACT

We have observed 19 Virgo cluster spiral galaxies with the Long Wavelength Spectrometer (LWS) onboard ESAs Infrared Space Observatory (ISO) obtaining spectra around the [CII] 157.741 μm fine structure line. These 19 galaxies are quiescent in star forming activity compared to previous studies from airborne observatories, sample RC3 types 0 to 5 and come from both the cluster core and the cluster periphery. The sample enables us to probe any difference in the [CII] emission between different RC3 types or between core and periphery galaxies.

Fourteen of the nineteen galaxies were detected in the [CII] line. Any influence of the Virgo cluster environment on the [CII] emission was found to be small compared with the strong dependence of the line emission on basic measurables such as morphology or bulk mass of the stellar component, as measured by the Near-IR (K′-band) luminosity. While the range of the [CII] to FIR ratio is less than in other surveys (reflecting the fact these galaxies are relatively quiescent), there is a good correlation between the strength of the [CII] line and the Far-IR flux, as measured by IRAS.

We find a trend of increasing [CII]-to-FIR flux ratio with increasing galaxy lateness. Moreover, the [CII]-to-K′-band flux ratio shows a one order of magnitude difference between RC3 type 0 and RC3 types later than 5. These two correlations express the relation between the mechanism of the [CII] emission and the massive star formation activity of the galaxy.

Key words: Galaxies: clusters: general – Galaxies: general – Galaxies: ISM – Infrared: galaxies

1 INTRODUCTION

The ISO (Kessler et al. 1996) Guaranteed Time programme VIRGO (Völk et al. *in prep*) is a study of a complete volume-limited, unbiased sample of spiral, irregular and BCD galaxies from the Virgo cluster, selected from the Virgo Cluster Catalogue (VCC) of Binggeli et al. (1985), as described in Boselli et al. (1997), using the ISOPHOT (Lemke et al. 1996) and ISOCAM (Cesarsky et al. 1996) instruments.

Selecting galaxies from a cluster represents the most convenient way of ensuring completeness in a wide variety of intrinsic properties, embracing a large dynamic range in star-formation activity. In particular, the Virgo cluster was chosen for several reasons: the high level of completeness of the VCC to B_T 18; at the distance to the cluster the typical angular sizes of the IR emitting regions are well matched to the angular resolution of ISO; the distance of the cluster was optimum for the detection of dwarf galaxies with ISOPHOT; and galaxies in the peripheral regions are thought to be freshly infalling from the field (Tully & Shaya 1984) and therefore less representative of the cluster environment.

While the VIRGO proposal is primarily photometric, we wished to observe many of these galaxies spectroscopically. Various constraints limited observations to the [CII] 157.741 μm cooling line. This line should probe photodissociation regions, cf Stacey et al. (1991), associated with massive star formation, and also the diffuse components of the Interstellar Medium, e.g. Nakagawa et al. (1998). It has

⋆ E-mail: kleech@iso.vilspa.esa.es

been observed not only in "compact" regions of the Galaxy like HII regions, OB associations, reflection nebulae, and planetary nebulae, but also in "diffuse" regions, as well as for entire galaxies, e.g. Madden et al. (1993). [CII] emission is thought to be the most important gas cooling process in normal, i.e. non-starburst, late type galaxies, balancing the photoelectric heating from grains.

While in field galaxies the [CII] line has a luminosity of the order of 10^{-3} to 10^{-2} that of the total FIR flux of a galaxy, e.g. Malhotra et al. (1997), the Virgo sample galaxies are less active in star forming activity, even at the top end of the luminosity range observed. Indeed the need to get a deep sample embracing quiescent galaxies was the fundamental motivation for observing Virgo galaxies.

At the distance of the Virgo cluster (taken to be 21 Mpc), the 70 arcsec diameter beam (Swinyard et al. 1998) of the LWS instrument (Clegg et al. 1996) covers an area of approximately 7 kpc in diameter – optical images of the Virgo galaxies by Sandage et al. (1985) indicate that the LWS beam covers out to the observed spiral arms. The extended [CII] emission detected at this distance in NGC 6946 by Madden et al. (1993) accounted for 70% of the total [CII] emission. Observation of Virgo galaxies with LWS will therefore detect not only [CII] emission from the dense nucleus but, assuming Virgo galaxies are similar to NGC 6946, will primarily sample the [CII] emission from diffuse regions in and between the spiral arms.

This paper presents a preliminary reduction, analysis and discussion of the [CII] data. Five VCC galaxies observed around the [CII] line by Smith & Madden (1997) are combined to produce a slightly larger sample. A further paper (Pierini et al. 1999) discusses the [CII] data in more detail and its relation to other measures of the star-forming activity. Modelling of the relation between [CII] line emission and star formation history of the present sample of galaxies is deferred to Pierini et al. *in prep.*

2 SAMPLE SELECTION AND OBSERVATIONS

The criteria for selecting the VIRGO sample galaxies are discussed in Völk et al. *in prep.* In particular, note that in order to provide a statistical check of the influence of the cluster environment on the far-infrared properties of galaxies, the selection was made from two contrasting regions, i.e. cluster core and cluster periphery, cf. Boselli et al. (1997).

LWS had the capability to detect the [CII] line in most of the spiral galaxies of the parent VIRGO sample, based on predictions from the IRAS fluxes and the average [CII] -line to FIR continuum ratios of late-type galaxies observed with KAO. Constraints on the available observing time, however, restricted us to a sample of 21 spirals earlier than Scd and complete to B_T = 12.3 mag. Of these 21 targets, the interacting pair VCC 1673 - 1676 was not included because the LWS beamwidth was not able to separate the individual emissions, and VCC 836 could not be observed as it was a target of another programme. The final 18 giant Virgo spirals nevertheless provide a sample of relatively quiescent galaxies in comparison to other samples of normal spiral galaxies selected for ISO observations e.g. Malhotra et al. (1997).

One other optically faint core galaxy, VCC 1326, was observed to serve as a cross-calibration target between the LWS measurements and the ISOPHOT measurements of the larger VIRGO programme. VCC 1326 is in some respects an atypical VCC galaxy as it is faint in the optical and yet is bright in the IR, so could be detected by LWS and PHOT. It was therefore selected to provide a useful photometric comparison between the LWS measurements and the PHOT measurements of Völk et al.

Information on all these galaxies is given in Table 1, together with the positions of reference fields to check for foreground [CII] emission from the Milky Way (denoted VBACK in the following tables and figures).

The observing log is given in Table 2. All observations carried out were standard LWS grating range scans (AOT 2's). Sets of observations were used to observe several galaxies in sequence (in ISO terminology, the observations were concatenated), with one sky background position used for each set. The observation set number is indicated in the table. All observations were made between 30^{th} June and 15^{th} July 1996 with no instrumental or satellite problems reported.

The performance of the LWS instrument is given in Clegg et al. (1996), in the ISOLWS Data Users Manual (Trams et al. 1998) and also in Swinyard et al. (1998). For the purpose of this paper, the most important instrumental characteristics to note are that at wavelengths around the [CII] line its spectral resolution is approximately 0.6 μm, or 1100 km/s, and that the instrumental beam profile is gaussian with a FWHM of approximately 70 arcsec.

3 DATA REDUCTION AND RESULTS

3.1 Data Reduction

The Auto Analysis Results from Off-Line Processing (OLP) version 7 were processed further using the ISO Spectral Analysis Package (ISAP) version 1.6 by: reading data in; discarding bad LWS data points; averaging scans for detector 8 (the one covering the 158 μm region); and finally fitting continua and gaussians to any lines seen in the data to obtain flux and central wavelength.

3.2 Results

Of the 19 galaxies observed, 14 were detected. Of the six background positions used, four had no detectable emission at galactic [CII] wavelengths, one has a possible detection and one was repointed to VCC 873, confirming the line flux and wavelength for that galaxy (it appears as the second VCC 873 observation in Tables 2 and 4). In the one possible background detection, the first observation on VBACK12, the line strength is very poorly determined and the linewidth is smaller than the instrumental resolution (a FWHM 200 km/s against an instrumental resolution of 1100 km/s) leading us to conclude that it is probably a noise spike we are seeing. In three galaxy observations (VCC 1110, 1326 and 1972) galactic [CII] emission was observed, and in all such cases was measured and noted. In all three cases the data were fit with a line at the wavelength of galactic [CII] and one at the expected position of the Virgo [CII] emission.

Line fluxes, central wavelengths and continuum fluxes

Table 1. *Sample galaxies and positions of selected reference fields.*

Target	Alternate name	RA (J2000)	DEC (J2000)	Core or Periphery	60 μm flux (Jy)	100 μm flux (Jy)	B_T	VCC Type	RC3 number
VCC 66	NGC 4178	12 12 46.9	10 52 07.0	P	2.8	9.0	11.9	SBc	5
VCC 92	NGC 4192,M98	12 13 48.4	14 54 07.2	P	6.5	21.5	10.9	Sb:	3
VCC 460	NGC 4293	12 21 13.2	18 23 03.6	P	4.6	10.6	11.2	Sa pec	1
VCC 857	NGC 4394	12 25 56.0	18 12 47.6	P	1.0	4.3	11.8	SBb	3
VCC 873	NGC 4402	12 26 06.8	13 06 47.6	C	5.4	17.4	12.6	Sc	5
VCC 1003	NGC 4429	12 27 26.2	11 06 30.3	C	1.4	4.3	11.1	S0/Sa pec	0
VCC 1043	NGC 4438	12 27 45.7	13 00 30.4	C	3.7	13.1	10.9	Sb(tides)	3
VCC 1110	NGC 4450	12 28 29.5	17 05 06.8	P	1.4	7.6	10.9	Sab pec	2
VCC 1158	NGC 4461	12 29 03.0	13 11 07.1	C	<0.2	<0.8	12.1	Sa	1
VCC 1253	NGC 4477	12 30 02.9	13 38 07.7	C	0.5	1.0	11.3	SB0/SBa	0
VCC 1326	NGC 4491	12 30 57.2	11 29 02.1	C	2.8	3.3	13.4	SBa	1
VCC 1412	NGC 4503	12 32 05.5	11 10 38.8	C	<0.2	1.0	12.1	Sa	1
VCC 1690	NGC 4569,M90	12 36 49.9	13 09 53.8	C	8.8	25.0	10.2	Sab	2
VCC 1727	NGC 4579	12 37 43.5	11 49 06.4	C	4.9	19.6	10.6	Sab	2
VCC 1813	NGC 4596	12 39 56.3	10 10 38.0	P	0.4	1.0	11.5	SBa	1
VCC 1869	NGC 4608	12 41 13.6	10 09 14.9	P	<0.2	<0.5	12.0	SB0/a	0
VCC 1972	NGC 4647	12 43 32.4	11 34 46.7	P	4.9	15.9	12.0	Sc	5
VCC 1987	NGC 4654	12 43 57.2	13 07 35.1	P	13.4	33.4	11.1	SBc	5
VCC 2070	NGC 4698	12 48 23.2	8 29 14.9	P	<0.2	1.6	11.5	Sa	1
VBACK01		12 13 30.9	15 30 47.2						
VBACK03		12 13 52.4	8 29 12.2						
VBACK04		12 25 05.9	17 43 52.1						
VBACK12		12 43 08.5	9 47 34.4						
VBACK13		12 48 14.5	12 58 38.7						

are given in Table 4. The errors quoted for the line and continuum fluxes are statistical, based on the ISAP results and do not include any errors due to, e.g., memory effects or absolute flux calibration errors, an indication of which can be found in Swinyard et al. (1998). A better guide to the flux errors can be obtained by comparing the two observations of VCC 873. The line fluxes agree to within the derived errors whereas the continuum fluxes differ by 15%. In cases where two gaussians are fit to a blended line the ISAP fitting routine does not produce an error estimate. In these cases the errors can be estimated by looking at similar flux cases where an error is quoted, and from this we estimate the errors to be of the order of 2×10^{-21} W/cm^2.

The continuum is quoted without subtracting any foreground emission from galactic emission. Given the wide variation in detected foreground continuum emission at the wavelength of [CII] (see VBACK observations in Table 4) and the fact the observed continuum emission from Virgo galaxies with detected [CII] emission is several times higher than any detected foreground continuum we have presented the data without any foreground continuum subtraction. Also note that the lines have not been resolved - linewidths are identical to the instrumental resolution.

Upper limits to the line fluxes are given for cases where no [CII] line was detected at the expected wavelength. These upper limits were derived from calculating the excess flux in a box of width 1100 km/s compared to the rest of the data range. The upper limit was set to be three times the standard deviation of this excess flux as the box was moved over the data range.

The [CII] line wavelength region for all galaxies and background positions are shown in figures 5 and 6. In both figures the baselines used during plotting are arbitrary, with the observed continuum levels given in Table 4. A few of the observations suffer from memory effects that cause the first few short-wavelength datapoints to be systematically lower than the continuum. These points were not used when deriving the line or continuum fluxes.

There is no difference, to within our measurement errors, between the velocities determined from optical data and those that can be determined from these [CII] measurements. The mean of the difference between the expected wavelength of the [CII] line and its observed wavelength is -0.01 μm, with a standard deviation of 0.03 μm, both significantly less than the LWS instrumental resolution of 0.6 μm.

4 DISCUSSION

As already said in the Introduction, our sample of 19 VCC late type galaxies is biased toward low current star formation activity galaxies. In order to increase the range in current SF activity, we add 5 low mass VCC galaxies observed by Smith & Madden (1997). A summary of the important information of these galaxies is given in Table 3.

4.1 The [CII] flux against FIR flux

Figure 1 shows the relation between the [CII] flux and the FIR flux from IRAS measurements given by $FIR = 1.26 \times$

Table 3. *Galaxies observed by Smith & Madden and added to this sample*

Target name	Alternate name	RC3 type	[C II] Line flux W/cm^2	60 μm flux(Jy)	100 μm flux(Jy)
VCC 89	NGC 4189	5	$9.1 \pm 0.8 \times 10^{-20}$	3.6	9.1
VCC 187	NGC 4222	7	$4.5 \pm 0.9 \times 10^{-20}$	1.1	3.3
VCC 465	NGC 4294	5	$8.4 \pm 0.9 \times 10^{-20}$	3.0	5.5
VCC 491	NGC 4299	6	$6.8 \pm 0.9 \times 10^{-20}$	2.7	4.7
VCC 1516	NGC 4522	5	$8.1 \pm 0.9 \times 10^{-20}$	1.6	4.7

Table 2. *Observing log.*

Target	Date Observed	Observation set	Observing time (s)
VCC 66	12 July	8	870
VCC 92	9 July	1	862
VCC 460	8 July	2	860
VCC 857	8 July	2	860
VCC 873	4 July	4	862
VCC 873[1]	4 July	4	1054
VCC 1003	5 July	5	860
VCC 1043	5 July	4	862
VCC 1110	8 July	2	862
VCC 1158	4 July	4	862
VCC 1253	4 July	4	862
VCC 1326	5 July	5	1054
VCC 1412	5 July	5	862
VCC 1690	5 July	4	861
VCC 1727	15 July	6	870
VCC 1813	15 July	6	870
VCC 1869	15 July	6	870
VCC 1972	15 July	6	870
VCC 1987	30 June	3	862
VCC 2070	15 July	7	870
VBACK01	9 July	1	860
VBACK03	12 July	8	1064
VBACK04	8 July	2	1054
VBACK12_1	15 July	6	1064
VBACK12_2	15 July	7	1064
VBACK13	30 June	3	1054

Note:
1. This was a repointed observation.

$10^{-18}(2.58 \times F_\nu(60\mu m) + F_\nu(100\mu m))Wcm^{-2}$ (Helou et al. 1988). Despite the spatial mis-match between the LWS 70 arcsec diameter circular aperture and the larger IRAS square apertures, there is a good correlation between these observed quantities within the approximately two orders of magnitude range in both observable quantities. We note that all the upper limits in the [CII] flux are found at the faint end of the FIR emission (i.e. at log FIR < -17.5).

When [CII] is detected, the [CII] to FIR ratio ranges from 0.1% to 0.5%. This covers the ranges expected for compact sources (0.2%), such as active star-forming regions, to the diffuse component on the ISM (0.6%) (Nakagawa et al. 1998). Galaxies observed by Stacey et al. (1991) cover the range 0.15 - 0.6%, and in NGC 5713 the ratio is 0.7% (Lord et al. 1996).

The tendency for the [CII] to FIR correlation to flatten off with increasing brightness, as observed by Stacey et al. (1991) for a sample embracing starburst and ultraluminous galaxies, is not apparent for the relatively quiescent Virgo sample. Moreover we observe that the low mass galaxies of Smith & Madden (1997) have higher [CII] fluxes than the quiescent galaxies in all cases.

4.2 Comparison with dust temperature

Figure 2 shows the [CII] to FIR ratio against the dust temperature, as measured by the ratio of the IRAS flux densities at 60 and 100 μm. The [CII]/FIR ratio is highest for galaxies with a 60 to 100 ratio of about 0.3 – 0.5, cf. Malhotra et al. (1997).

Of interest in this plot VCC 1326 with 60/100 of 0.85 but an apparently anomalously low [CII]/FIR ratio of 0.09%. Moreover, there is the possibility that the [CII] emission from VCC 1326 is confused with that from galactic foreground emission, making the [CII]/FIR ratio even lower. This observation, however, is one of the few where we deconvolved the Virgo galaxy [CII] emission from galactic emission, and its [CII] emission is several times that the average foreground. We therefore do not expect the measurement to be significantly contaminated by galactic [CII] emission. This low [CII]/FIR ratio is extreme for our sample, but is within the range of observed values in Malhotra et al. (1997) – note however that the galaxies in their sample at such high values of 60/100 are probably starburst galaxies. VCC 1326 is the faintest galaxy in our sample, with a B_T magnitude of 13.4, but as we noted in section 2 it is a somewhat atypical VCC galaxy being IR bright. Interestingly, it has enhanced X-ray emission with respect to the hot Intracluster Medium (Ohashi & Kikuchi 1997). Why this galaxy lives in an otherwise unpopulated region of this diagram is unknown unless it is a starburst galaxy – optical spectroscopy will be needed to determine this. However, from the comparison of the K′-band image (Boselli et al. 1997) and the Hα image (Hippelein et al. *in prep*) we note that the Lyman emission is centrally peaked.

4.3 [CII] and morphological type

Figure 3 shows the [CII]/FIR ratio against RC3 type. Ignoring the upper limits, there is marked difference between the ratio for RC3 types 0 - 3 against RC3 types later than 5. Galaxies which have higher continuum and line brightness

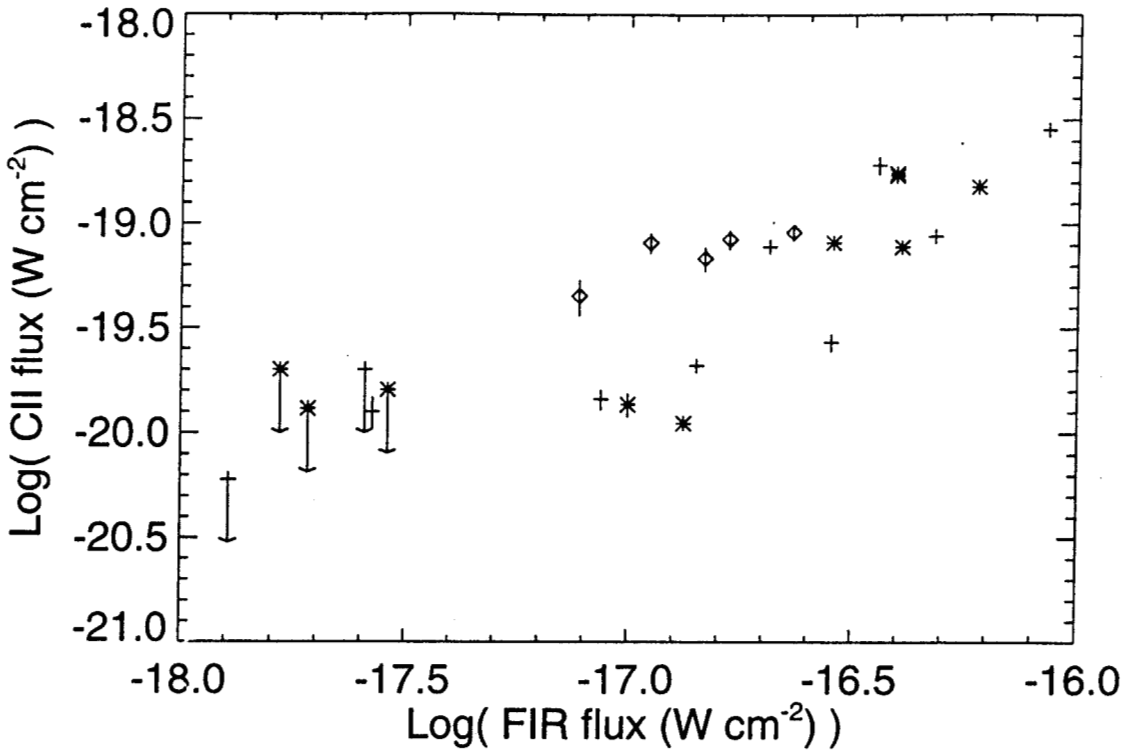

Figure 1. [CII] flux against FIR flux. Error bars are marked in the vertical, where they are larger than the symbol size, and upper limits are marked. Core galaxies are marked by '*', periphery by '+' and galaxies from Smith & Madden by diamonds.

tend to have later Hubble types. Since massive star formation activity increases with increasing lateness, e.g. Kennicutt et al. (1994), we interpret this correlation as a proof in favour of the model of gas-heating produced by the photoelectric effect on dust grains, induced by hard UV photons from intermediate mass ($5 \leq M \leq 20\ M_{\odot}$) stars – cf. Tielens & Hollenbach (1985) and Pierini et al. (1999).

If the [CII] flux is normalised by K′-band ($\lambda = 2.1$ micron) flux, a measure of the number of old stars in the galaxy which constitute the bulk of the stellar mass component, this difference with RC3 type is even more pronounced, as can be seen from figure 4. This mass-normalization removes simple scaling effects in the relation between the [CII] and the K′-band luminosities (not shown).

Conversely, there is no apparent relation between the [CII] line properties and position in the cluster from figures 1, 2, 3 and 4. Neither is there evidence for a relation between the [CII] line properties and HI mass surface density, from Warmels (1988), in the galaxian disks. Therefore, any relation of the [CII] emission to the diffuse HI component of the ISM is not obvious, at least for the central regions of the disks observed.

5 CONCLUSION

We have observed nineteen Virgo cluster member late type galaxies with the LWS spectrometer onboard the ISO satellite around the [CII] fine structure line, detecting [CII] emission in fourteen of these. A good correlation is found between the strength of the [CII] and the FIR flux. Moreover, we find evidence for a dependance of the [CII]-to-FIR flux ratio on the galaxy morphology, with the [CII]/FIR ratio increasing with later Hubble types. A stronger correlation with lateness is found for the [CII]-to-K′-band flux ratio, the K′ flux representing the bulk of the stellar mass content of the galaxy. Since lateness is correlated to massive star formation activity, we interpret these two relations as evidence of the model of gas heating through the photoelectric effect on dust grains, induced from hard UV emission from intermediate mass stars.

Finally, we find that one galaxy, VCC 1326, lies in the region of the [CII]/FIR vs. 60/100 plane populated by starburst galaxies.

REFERENCES

Binggeli B., Sandage A., Tamman G.A., 1985, AJ 90, 1681

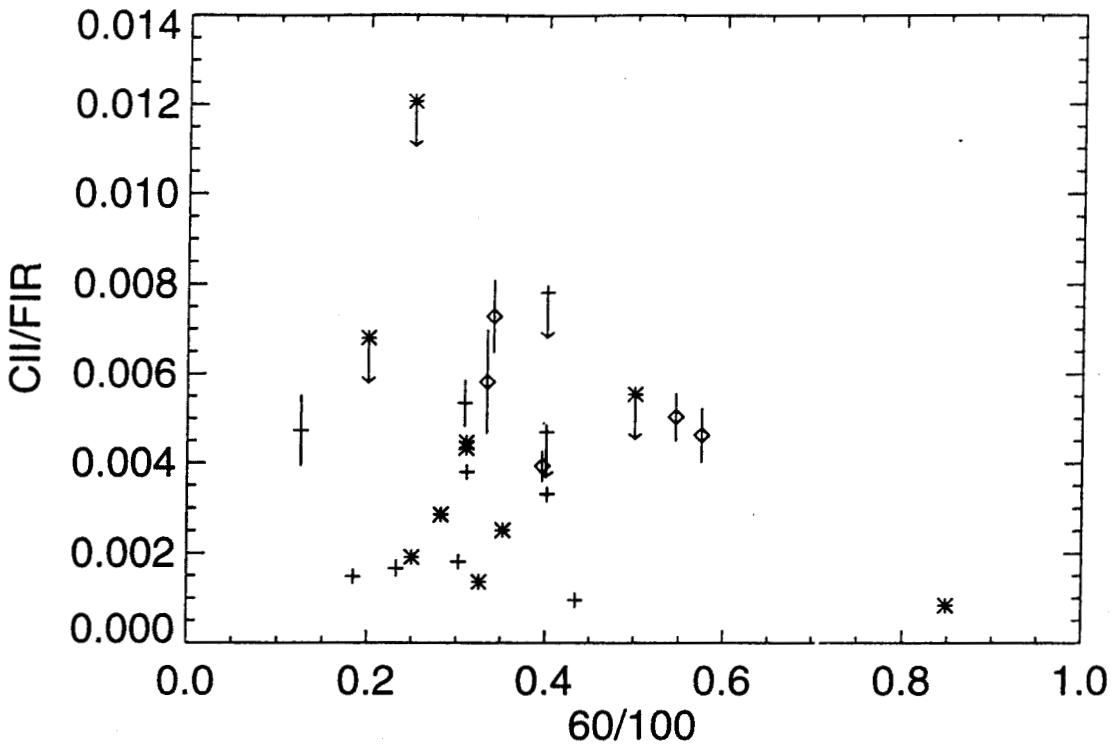

Figure 2. [CII]/FIR ratio against dust temperature, indicated by 60/100 μm ratio. Error bars and upper limits are marked. Core galaxies are marked by '*', periphery by '+' and galaxies from Smith & Madden by diamonds.

Boselli A., Tuffs R.J., Gavazzi G., Hippelein H., Pierini D., 1997, A&AS 121, 507
Cesarsky C.J. et al. 1996, A&A 315, L32
Clegg P.E et al. 1996, A&A 315, L38
Helou G., Khan I.R., Malek L., Boehmer L., 1988, ApJS 68, 151
Kennicutt R.C., Tamblyn P., Congdon C., 1994, ApJ 435, 22
Kessler M.F. et al. 1996, A&A 315, L27
Lemke D. et al. 1996, A&A 315, L64
Lord S.D. et al. 1996, A&A, 315, L117
Madden S.C., Geis N., Genzel R., Herrmann F., Jackson J., Poglitsch A., Stacey G.J., Townes C.H., 1993, ApJ 407, 579
Malhotra S., et al. 1997, ApJ 491, L27
Nakagawa T., et al. 1998, ApJS 115, 259
Ohashi T., Kikuchi K. 1997, IAU 188, 148
Pierini D., Leech K.J., Tuffs R.J., Völk, H.J, 1999, MNRAS 303, L29
Sandage A., Binggeli B., Tammann G.A. 1985, AJ 90, 395
Smith B.J., Madden S.C., 1997, AJ 114, 138
Stacey G.J., Geis N., Genzel R., Lugten J.B., Poglitsch A., Sternberg A., Townes C.H., 1991, ApJ 373, 423
Swinyard B., Burgdorf M., Clegg P.E., Davis G.R., Griffin M.J., Gry C., Leeks S.J., Lim T.L., Pezzuto S., Tommasi E., 1998, In Proc. of SPIE Conference on Infrared Astronomical Instrumentation, Kona, Hawaii, SPIE Vol. 3354 pp 888-899
Tielens A.G.G.M., & Hollenbach D., 1985, ApJ 291, 722
Trams N., et al. 1998, ISOLWS Data Users Manual, SAI/95-219/Dc, http://www.iso.vilspa.esa.es/manuals/lws_idum5/
Tully R.B., Shaya E.J., 1984, ApJ, 281, 31
Warmels R.H., 1988, A&AS 72, 427

ACKNOWLEDGEMENTS

This paper is based on observations with the Infrared Space Observatory (ISO). ISO is an ESA project with instruments funded by ESA member states (especially the PI countries: France, Germany, the Netherlands and the United Kingdom) and with the participation of ISAS and NASA.

The ISO Spectral Analysis Package (ISAP) is a joint development by the LWS and SWS Instrument Teams and Data Centres. Contributing institutes are CESR, IAS, IPAC, MPE, RAL and SRON.

This paper has been produced using the Royal Astronomical Society/Blackwell Science LaTeX style file.

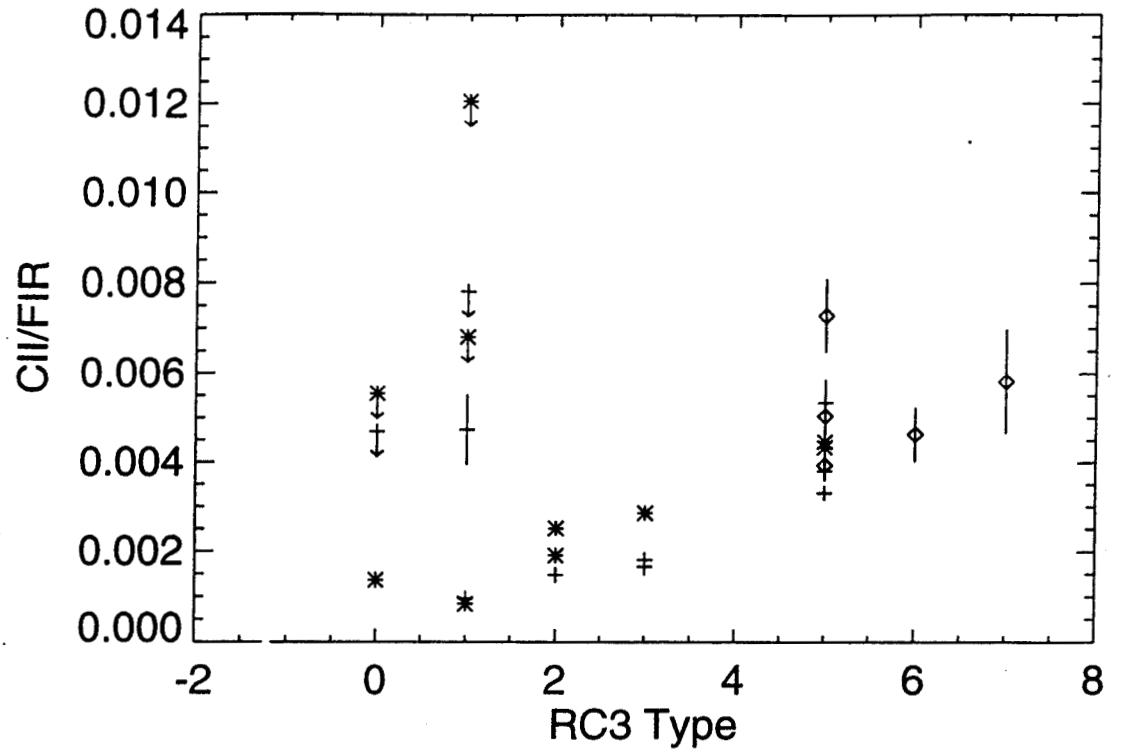

Figure 3. [CII]/FIR ratio against RC3 Type. Error bars and upper limits are marked. Core galaxies are marked by '*', periphery by '+' and galaxies from Smith & Madden by diamonds.

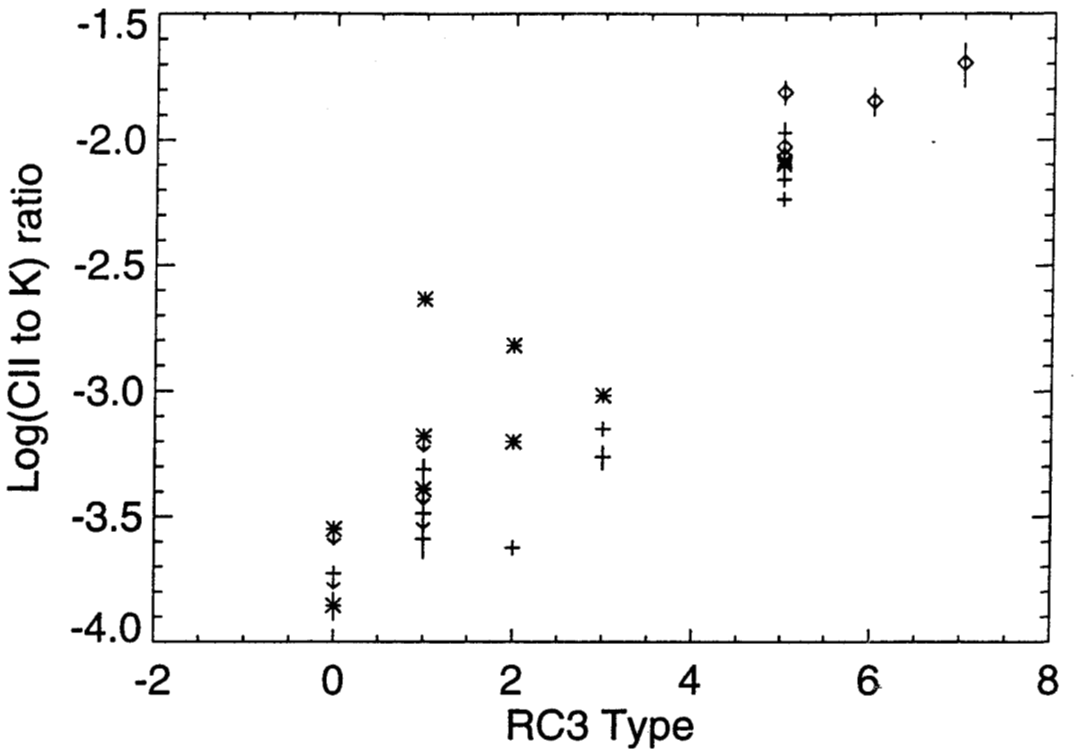

Figure 4. [CII]/K′ flux ratio against RC3 Type. The difference between RC3 types 0 and 5 are more marked when the [CII] flux is normalised by a crude measure of the number of old stars. Error bars and upper limits are marked. Core galaxies are marked by '*', periphery by '+' and galaxies from Smith & Madden by diamonds.

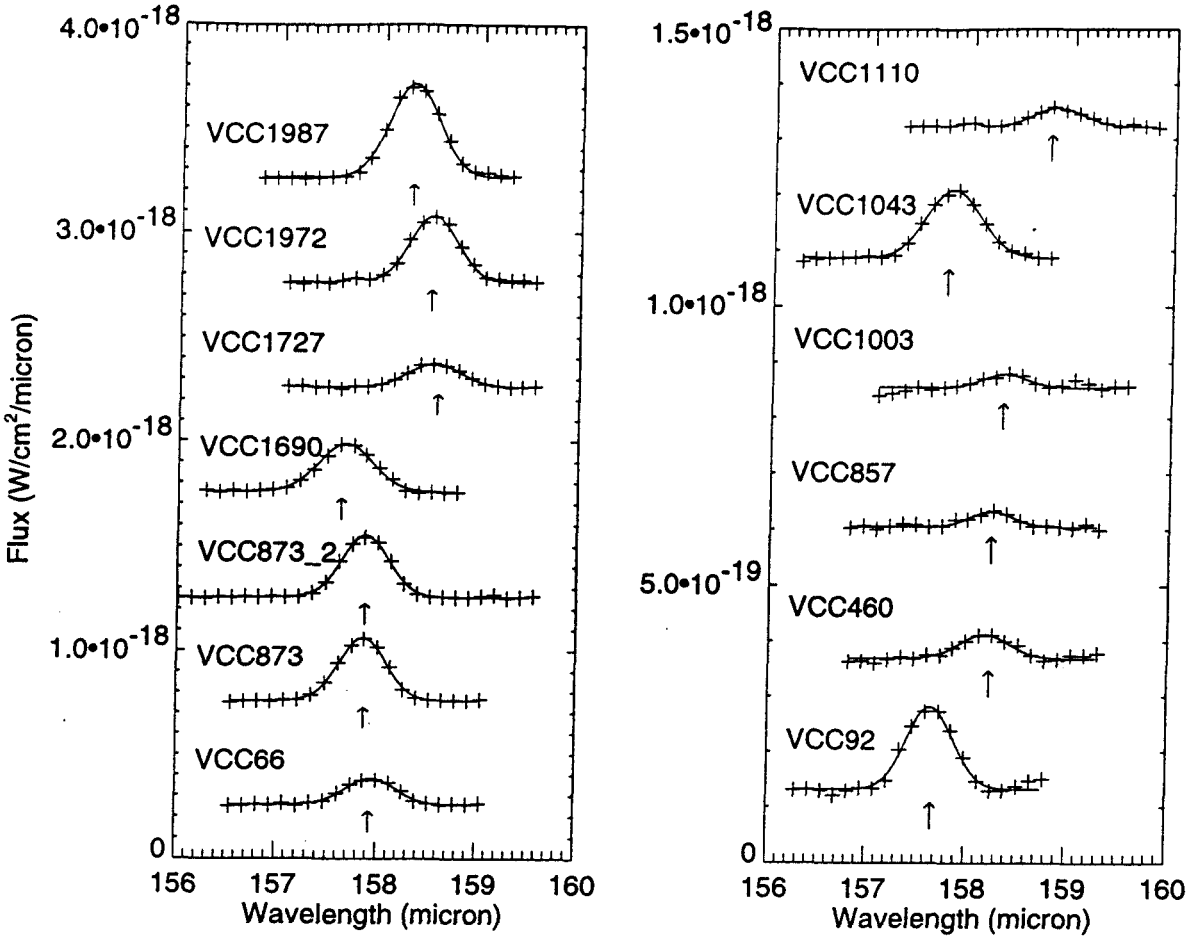

Figure 5. Virgo galaxy observations. The baselines are arbitrary but can be derived from Table 4. The expected position of the [CII] emission line is marked by an arrow.

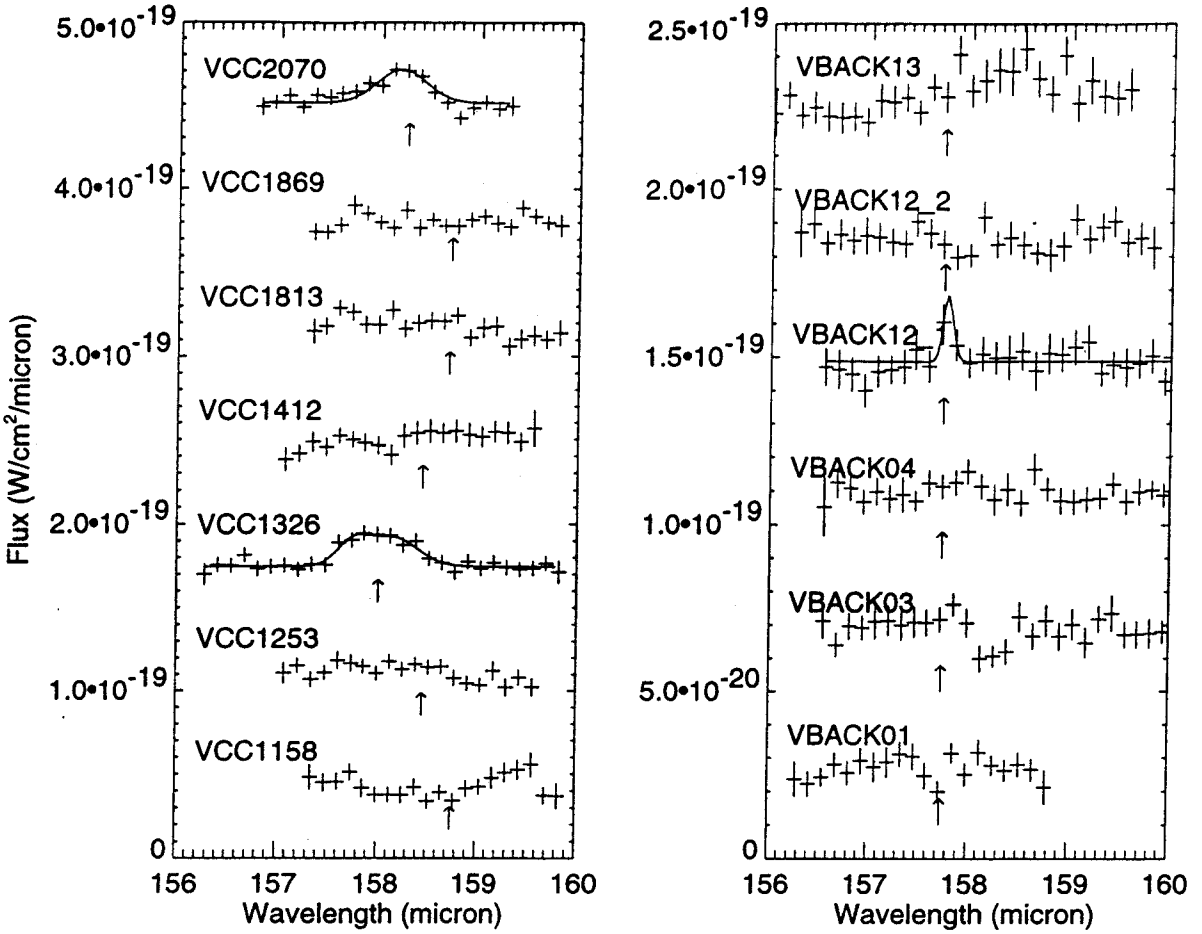

Figure 6. Virgo galaxy and background observations. The baselines are arbitrary but can be derived from Table 4. The expected position of the [CII] emission line is marked by an arrow.

Table 4. *Observation Results*

Target name	Continuum flux $W/cm^2/\mu m$	Line FWHM km/s	Line flux W/cm^2	Line Wavelength μm	Note
VCC 66	$6.7 \pm 0.2 \times 10^{-20}$	1100	$7.8 \pm 0.3 \times 10^{-20}$	157.943 ± 0.008	
VCC 92	$1.73 \pm 0.02 \times 10^{-19}$	1000	$8.8 \pm 0.4 \times 10^{-20}$	157.653 ± 0.008	
VCC 460	$1.16 \pm 0.01 \times 10^{-19}$	1100	$2.7 \pm 0.3 \times 10^{-20}$	158.18 ± 0.02	
VCC 857	$6.42 \pm 0.08 \times 10^{-20}$	1000	$1.4 \pm 0.2 \times 10^{-20}$	158.23 ± 0.02	
VCC 873	$2.10 \pm 0.02 \times 10^{-19}$	1000	$1.76 \pm 0.04 \times 10^{-19}$	157.849 ± 0.004	
VCC 873[1]	$1.80 \pm 0.02 \times 10^{-19}$	1000	$1.71 \pm 0.04 \times 10^{-19}$	157.866 ± 0.004	
VCC 1003	$5.0 \pm 0.1 \times 10^{-20}$	1000	$1.4 \pm 0.2 \times 10^{-20}$	158.34 ± 0.02	
VCC 1043	$1.13 \pm 0.01 \times 10^{-19}$	1200	$8.2 \pm 0.2 \times 10^{-20}$	157.805 ± 0.005	
VCC 1110	$7.1 \pm 0.1 \times 10^{-20}$	1100	2.1×10^{-20}	158.83 ± 0.06	
		400	1.7×10^{-21}	157.94 ± 0.04	g
VCC 1158	$2.3 \pm 0.0 \times 10^{-20}$		$< 2 \times 10^{-20}$		
VCC 1253	$2.3 \pm 0.0 \times 10^{-21}$		$< 1.6 \times 10^{-20}$		
VCC 1326	$3.9 \pm 0.2 \times 10^{-20}$	1100	1.3×10^{-20}	158.1 ± 0.3	
		700	5.0×10^{-21}	157.741	g
VCC 1412	$2.6 \pm 0.0 \times 10^{-20}$		$< 1.3 \times 10^{-20}$		
VCC 1690	$2.56 \pm 0.02 \times 10^{-19}$	1200	$1.51 \pm 0.04 \times 10^{-19}$	157.676 ± 0.005	
VCC 1727	$1.23 \pm 0.02 \times 10^{-19}$	1200	$7.8 \pm 0.3 \times 10^{-20}$	158.531 ± 0.008	
VCC 1813	$3.1 \pm 0.0 \times 10^{-20}$		$< 2 \times 10^{-20}$		
VCC 1869	$4.9 \pm 0.0 \times 10^{-21}$		$< 6 \times 10^{-21}$		
VCC 1972	$2.39 \pm 0.04 \times 10^{-19}$	1100	1.9×10^{-19}	158.5 ± 0.2	
		400	3.7×10^{-21}	157.7 ± 0.4	g
VCC 1987	$2.97 \pm 0.04 \times 10^{-19}$	1100	$2.84 \pm 0.07 \times 10^{-19}$	158.289 ± 0.004	
VCC 2070	$4.5 \pm 0.1 \times 10^{-20}$	1100	$1.3 \pm 0.2 \times 10^{-20}$	158.18 ± 0.03	
VBACK01	$2.19 \pm 0.0 \times 10^{-20}$		$< 5 \times 10^{-21}$		
VBACK03	$-1.8 \pm 0.0 \times 10^{-21}$		$< 1.0 \times 10^{-20}$		
VBACK04	$2.0 \pm 0.0 \times 10^{-20}$		$< 6 \times 10^{-21}$		
VBACK12_1[2]	$1.5 \pm 0.4 \times 10^{-21}$	200	$3 \pm 2 \times 10^{-21}$	157.78 ± 0.02	
VBACK12_2	$1.3 \pm 0.0 \times 10^{-21}$		$< 7 \times 10^{-21}$		
VBACK13	$7.1 \pm 0.0 \times 10^{-22}$		$< 2.5 \times 10^{-20}$		

Notes:
1. This was a repointed observation.
2. This is probably a noise spike – see section 3.2
g galactic [CII] emission.

From: Tom Jarrett
Date: Fri Mar 19 14:39 PST 1999
To: vandyk
Subject: abell clusters

here's some:
AB_1589
AB_2151
AB_1991
AB_1960
AB_2009
AB_2017
AB_2089
AB_2065
AB_2142